

Motion of tethered instrumentation platforms for acoustic Doppler velocimetry in energetic tidal flows

Samuel Harding^{a,*}, Levi Kilcher^b, Jim Thomson^c

^a*Pacific Northwest National Laboratory, Richland, Washington, USA*

^b*National Renewable Energy Laboratory, Golden, Colorado, USA*

^c*Applied Physics Laboratory, University of Washington, Seattle, Washington, USA*

Abstract

The deployment of acoustic Doppler velocimeters (ADVs) on tethered instrumentation platforms has recently been investigated for the characterization of turbulence for the emerging tidal energy industry. A variety of instrumentation platforms have been deployed as part of this work including the streamlined StableMoor™ buoy (SMB), the Tidal Turbulence Mooring (TTM) system based on a conventional 0.9 m spherical buoy, and a 100 lb sounding weight. The first two systems are bottom mounted moorings and the latter is deployed from a research vessel. The motion-induced velocities at the ADV head on each platform type and instrument configuration are discussed in the context of flow energies relevant to tidal energy and with the objective of reducing motion contamination of measurements.

The SMB with a single ADV head mounted on the nose provided the most stable platform for the measurement of tidal turbulence in the inertial sub-range for flow speeds exceeding 1.0 ms^{-1} . The modification of the SMB with a transverse wing configuration for multiple ADVs showed a similar frequency response to the nose configuration but with large contamination in the vertical direction as a result of platform roll. While the TTM provided a relatively stable configuration at low frequencies of motion, the motion-induced velocity at the ADV head became significant at frequencies above $f > 1 \text{ Hz}$. The sounding weight measurements showed the greatest motion at the ADV head but are likely to be influenced by both prop-wash and vessel motion.

*Corresponding author

Email address: samuel.harding@pnnl.gov (Samuel Harding)

Keywords: Tidal turbulence, Tethered platform, ADV, Tidal energy

1 1. Introduction

The kinetic energy of tidal currents presents a valuable source of renewable energy. For this application, the understanding of the flow behavior is critical to the design and operation of a tidal energy conversion device. The interest in understanding mid-water oceanic turbulence also extends to the fields of marine microbiology, ecology, mooring technologies, thermal mixing and chemical stratification. Though the mean kinetic energy and bulk turbulence statistics of a tidal site can be characterized with relative ease using acoustic Doppler current profilers (ADCPs), the higher temporal and spatial resolution required to detect the full range of turbulent scales in an energetic tidal site poses a greater measurement challenge.

Understanding the turbulence characteristics at the hub depth of the marine hydro-kinetic (MHK) device is of particular interest. This is the location where the flow is ultimately converted from kinetic energy to electricity, and so the fluctuating component of the flow is not only manifested in unsteady hydrodynamic loading conditions (McCann, 2007; Milne et al., 2010; Afgan et al., 2013), but also in the energy output.

A wide range of MHK concepts are currently in development, however many concepts reflect the common depth profiles which indicate that the peak available energy is found at mid-depths of the vertical velocity profile (Legrand, 2009). Locations close to the seabed exhibit lower flow speeds due to the flow shear created by friction forces. Hub heights approaching the free surface are susceptible to the unpredictable meteorologically-driven surface dynamics. It follows that the typical energy extraction location of an MHK device is difficult to physically access from either fixed bottom-mounted or vessel-mounted deployments prior to prototype installations.

Many key properties of tidal turbulence are able to be directly characterized by high frequency point velocity measurements. This is most widely achieved in the field through the use of an acoustic Doppler velocimeter (ADV), which uses a bi-static configuration of transmitters and receivers to measure a sample volume of approximately 1 cm^3 with high temporal resolution.

The challenge with deploying a point-measurement velocimeter is accessing the areas of interest in the water column. Large hydrodynamic loads and

35 moments are generated on structures which are fixed to the ocean floor or
36 penetrate from the surface. These moments can be mitigated through the use
37 of compliant mooring lines to submerged instrumentation. With the removal
38 of fixed structures under moored configurations, the motion of the instru-
39 ment relative to the motion of the water can become significant (Thomson
40 et al., 2013; Paskyabi and Fer, 2013; Matt et al., 2014).

41 Meaningful velocity measurements of tidal turbulence can be achieved
42 through the measurement and removal of the platform motion from the mea-
43 sured velocity (Kilcher et al., 2014a; Thomson et al., 2013, 2014). In this
44 process, the motion of submerged instrumentation platforms are measured
45 using inertial measurement units (IMUs), to detect both the linear acceler-
46 ation in the earth coordinate frame as well as the angular rotation rate in
47 pitch, roll and yaw.

48 Persistent motion contamination is observed when the motion-induced
49 velocity at the ADV head was large. The motion contamination can thus be
50 minimized through the selection of the most stable platform for the veloc-
51 ity measurements. In short, ‘the best form of motion correction is motion
52 prevention’ (Jim Thomson, pers. comm.). This paper presents the motion-
53 induced velocity at the ADV head mounted on a range of sub-sea platform
54 geometries and configurations which were deployed in work presented by
55 Kilcher et al. (2015) in Part 1 of this paper. This approach is similar to that
56 used in the motion-correction of shipboard atmospheric measurements, such
57 as those presented by (Edson et al., 1998).

58 As an appendix to this work, the platform motion over a wide range of
59 frequencies is calculated by combining the low frequency bottom tracking
60 capabilities of an ADCP with the high frequency IMU measurements.

61 **2. Instrumentation**

62 *2.1. Inertial measurement units*

63 The IMU used in the following experiments is the LORD MicroStrain
64 3DM-GX3-25-OEM inertial sensor (LORD MicroStrain, 2014). This unit
65 is a industrial grade attitude heading and reference system (AHRS) with
66 integrated magnetometers, with a form factor of $38 \times 24 \times 12$ mm. The IMU
67 was integrated into the Nortek Vector ADVs with tight time synchronization,
68 with the unit axes orthogonal to the axes of the ADV body (pressure case).

69 The calculation of the ADV head motion from the IMU output is pre-
70 sented in Part 1 of this paper (Kilcher et al., 2015).

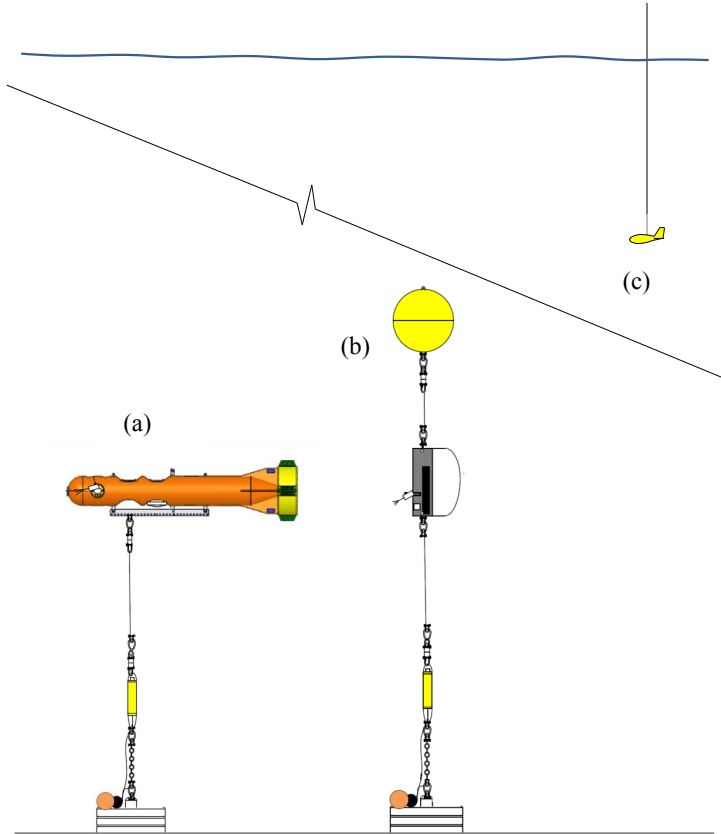


Figure 1: Platform schematics: (a) StableMoor™ buoy (SMB), (b) Tidal Turbulence Mooring system (TTM) and (c) sounding weight tethered to the research vessel.

71 2.2. *Mooring hardware*

72 Three instrumentation platforms for ADV deployments were considered in
 73 this motion comparison analysis. Each platform is introduced in the following
 74 subsections. A schematic of all three platforms is shown in Figure 1 with key
 75 parameters summarized in Table 1.

76 2.2.1. *StableMoor™ buoy platform*

77 The streamlined StableMoor™ mooring buoy (SMB) is an instrumenta-
 78 tion platform produced by DeepWater Buoyancy, Inc. (formerly designed
 79 by Flotation Technologies). The buoy is manufactured using syntactic foam
 80 with a protective GRP shell. The elongated form of the buoy and GRP

Table 1: Velocimetry platform properties.

Platform	Fastening location	Streamwise platform length (m)	Line length, L (m)	Dry mass, m (kg)	Submerged mass ¹ (kg)
SMB	Seabed	3.6	9.5	-	-180
TTM	Seabed	0.9	11	137	-300
Sounding weight	Vessel	0.4	20, 30, 40	45	41

¹ Negative values indicate net buoyancy

81 tail vane are designed to reduce drag loads and increase dynamic stability in
 82 energetic flow conditions.

83 In this study, ADVs were mounted to the SMB in two configurations,
 84 both with the ADV head in the upward looking direction:

85 • Winged-mode: A carbon-fiber beam with an elliptical cross-section was
 86 installed near the nose of the SMB with a port and starboard ADV
 87 attached to either end, as shown in Figure 2a. The ADV bodies were
 88 installed in the instrumentation wells in the SMB body.

89 • Nose-mode: The carbon-fiber beam was removed and a single ADV was
 90 installed, with the ADV head attachment protruding from the nose of
 91 the SMB, as shown in Figure 2b.

92 2.2.2. Tidal Turbulence Mooring platform

93 The Tidal Turbulence Mooring (TTM) system uses two ADVs are mounted
 94 to a vane which is then fixed to a mooring line between an anchor on the
 95 seabed and a 0.9 m spherical buoy. This is the same configuration as used in
 96 previous experiments by Thomson et al. (2013). The principal components
 97 of the TTM are shown in Figure 3.

98 2.2.3. Sounding weight platform

99 The sounding weight used in these experiments is a streamlined instru-
 100 mentation platform is suspended below the research vessel. The 100 lb USGS
 101 ‘Columbus-type’ weight is cast from lead, with aluminum tail fins. A davit
 102 was used to deploy the sounding weight over the port side of the vessel as

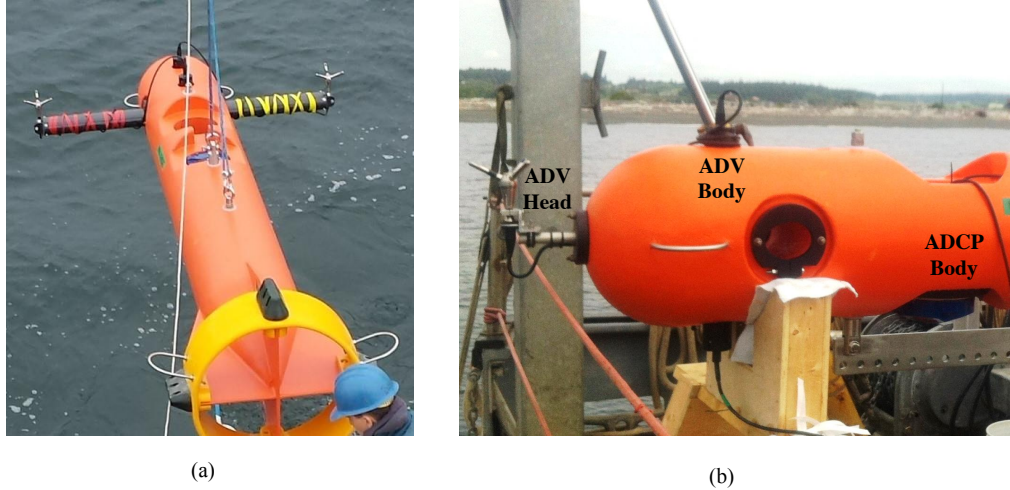


Figure 2: StableMoor™mooring buoy configurations: a) Two ADVs in winged-mode and b) a single ADV in nose mode.

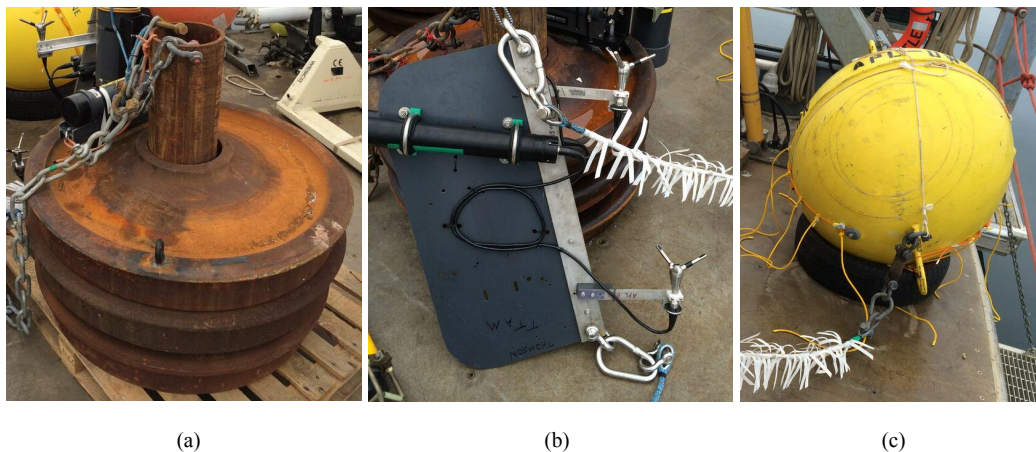


Figure 3: TTM components: a) Seabed anchor constructed using three railroad wheels, b) two ADVs on strong-back vane attached to mooring line and c) spherical buoy at end of mooring line.

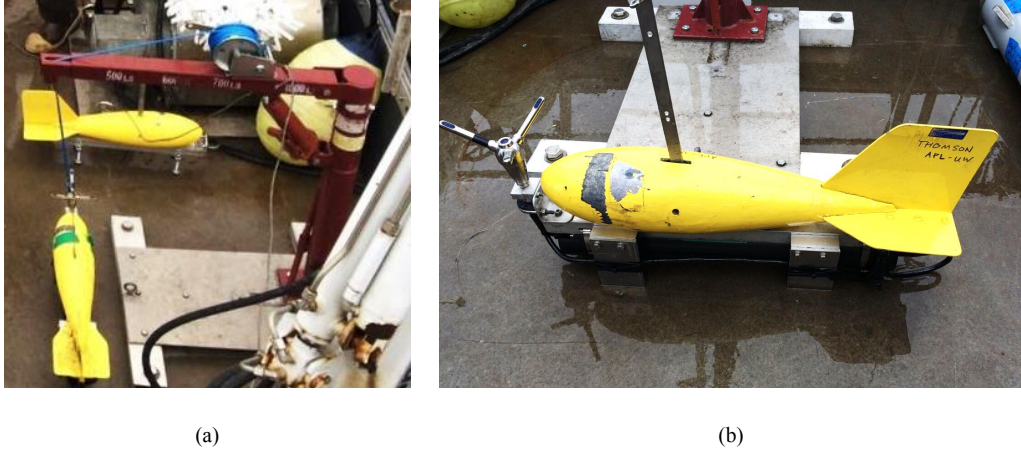


Figure 4: Sounding weight platform: a) sounding weight tethered to davit for vessel mounted deployment and b) ADV head configuration.

103 shown in Figure 4a. The cabled ADV head was installed in an upwards look-
104 ing orientation at the nose of the sounding weight, as shown in Figure 4b.

105 3. Coordinate System

106 The linear and angular motion of the each platform is measured by the
107 IMU in the mounted ADV body and the motion correction is performed in
108 the earth coordinate frame. All velocity signals are then rotated into a right-
109 handed platform coordinate system such that $\vec{u}_m^p(t) = (v_1, v_2, v_3)$ where v_1 is
110 aligned with the longitudinal axis of the platform (positive towards nose), v_2
111 is the transverse direction and v_3 is aligned in the vertical direction (positive
112 up).

113 Performing the platform motion characterization in the principal coordi-
114 nate system (aligned with the principal flow direction) caused cross contami-
115 nation between the motion signal in the stream-wise and cross-flow directions
116 at this site. This is due to the asymmetry in the ebb and flood flow direc-
117 tion at the deployment location (Polagye and Thomson, 2013). Some level
118 of directional asymmetry is often observed in tidal flows, and for this reason
119 the authors suggest the use of platform coordinates in such motion analysis.

120 The motion-induced velocity measured by the ADV, ($\vec{u}_m(t)$), is com-
121 puted from the IMU rotation rate vector ($\vec{\omega}$) and the linear acceleration

122 vector (\vec{a}') using Equation 1.

$$\vec{u}_m(t) = \vec{\omega}(t) \times \vec{l} + \int \vec{a}'(t) dt \quad (1)$$

123 Here l is the vector from the IMU to the ADV sensor-head and \vec{a}' is the
124 high-pass filtered IMU acceleration. For more details on this process, refer
125 to Part 1 of this paper by Kilcher et al.

126 4. Motion-induced velocity results

127 4.1. Frequency response

128 The motion-induced velocity measured by the ADV is presented in the
129 frequency domain in the same way as TKE spectra are present for the flow
130 in which they are deployed. Specifically, spectra are calculated using a fast
131 Fourier transform (\mathcal{F}) of the motion-induced ADV velocity was calculated
132 using 128 s of detrended, hanning-windowed segments with 50% overlap, such
133 that $S\{u\}(f) = |\mathcal{F}(u)|^2$.

134 The frequency response amplitude, $H\{\vec{u}\}(f)$, relates the TKE spectra,
135 $S\{\vec{u}\}(f)$, (presented in Part 1) to the energy spectra of the motion-induced
136 velocity at the ADV head, $S\{\vec{u}_m\}(f)$, as defined in Equation 2. This method
137 is analogous to the processing of the frequency response amplitude of a signal.

$$H\{\vec{u}^p\}(f) = \frac{S\{\vec{u}_m^p\}(f)}{S\{\vec{u}^p\}(f)} \quad (2)$$

138 The frequency response function in the direction of the longitudinal,
139 transverse and vertical axis of the platform are denoted as $H\{v_1\}, H\{v_2\}$
140 and $H\{v_3\}$, respectively.

141 Persistent motion contamination was observed when the frequency re-
142 sponse amplitude was large. At these frequencies the velocity correction
143 process was not able to totally remove the motion-induced velocity at the
144 ADV head, resulting in irregularities in $S\{\vec{u}^p\}(f)$. The velocity spectra
145 were interpolated across the contaminated frequencies before calculation of
146 the frequency response in Equation 2 to avoid the propagation of errors. For
147 this reason the frequency response amplitude has been used in this analysis
148 rather than the conventional transfer function definition¹ as the motion con-

¹Defined as the ratio between the cross-power spectral density of the motion-induced velocity and the flow velocity, and the power spectral density of the velocity

149 tamination was not able to be removed from the cross power spectral density
150 term.

151 *4.1.1. StableMoor™ buoy*

152 The motion-induced ADV energy spectra is presented in Figure 5 for all
153 tested ADV configurations. This figure groups the velocity spectra in terms
154 of the mean flow velocity, U , in increments of 0.5 ms^{-1} .

155 The motion-induced ADV velocity for the starboard and port instruments
156 in winged mode (top and middle plots in Figure 5, respectively) demonstrated
157 very similar motion characteristics, with the majority of the motion energy
158 is found in the frequency range of 0.07-0.2 Hz. In general, the motion of the
159 instrument increases at higher mean flow velocities. The frequency response
160 amplitude is very similar between the two configurations in all directions for
161 $f \leq 0.3 \text{ Hz}$. In this low frequency range, the motion is predominantly in
162 the lateral direction. The motion can be visualized as a ‘swimming’ dynamic
163 where the platform yaws about the z -axis. The peak energy spectra of the
164 motion-induced velocity at the ADV head, $S\{v_2\}(0.07 \text{ Hz}) \approx 0.1 \text{ m}^2\text{s}^{-2}\text{Hz}^{-1}$.
165 The period of this motion is 14 s with an amplitude of approximately 0.7 m.

166 A natural frequency phenomena is observed at 0.8 Hz in the transverse
167 and vertical directions at low flow speeds, with a maximum response in the
168 $0.5 < U \leq 1.0 \text{ ms}^{-1}$ velocity band. The frequency response was calculated for
169 the mean velocity range where the high frequency resonance was observed,
170 $0 < U \leq 1.0 \text{ ms}^{-1}$. Figure 6 shows the key dynamics of the SMB motion for
171 the winged configuration (port ADV) and nose configuration.

172 The higher frequency resonance is observed in the frequency response
173 amplitude for the transverse motion and also observed in vertical direction
174 in winged mode. As the SMB moves in the lateral direction, the mooring
175 line fastened to the underside of the buoy causes a rolling motion at the
176 same frequency. In the case of the winged configuration, the angular velocity
177 of the roll is translated into a vertical motion of the ADV heads which are
178 mounted on a horizontal moment arm. This introduces a strong rotation-
179 induced vertical velocity at the same frequency as the lateral motion, at
180 $f = 0.8 \text{ Hz}$.

181 *4.1.2. Tidal Turbulence Mooring*

182 The motion-induced ADV velocity in the TTM configuration is a func-
183 tion of two dynamic phenomena. Firstly, the motion of the spherical buoy
184 dominates the motion of the system at the natural frequency of the pendular

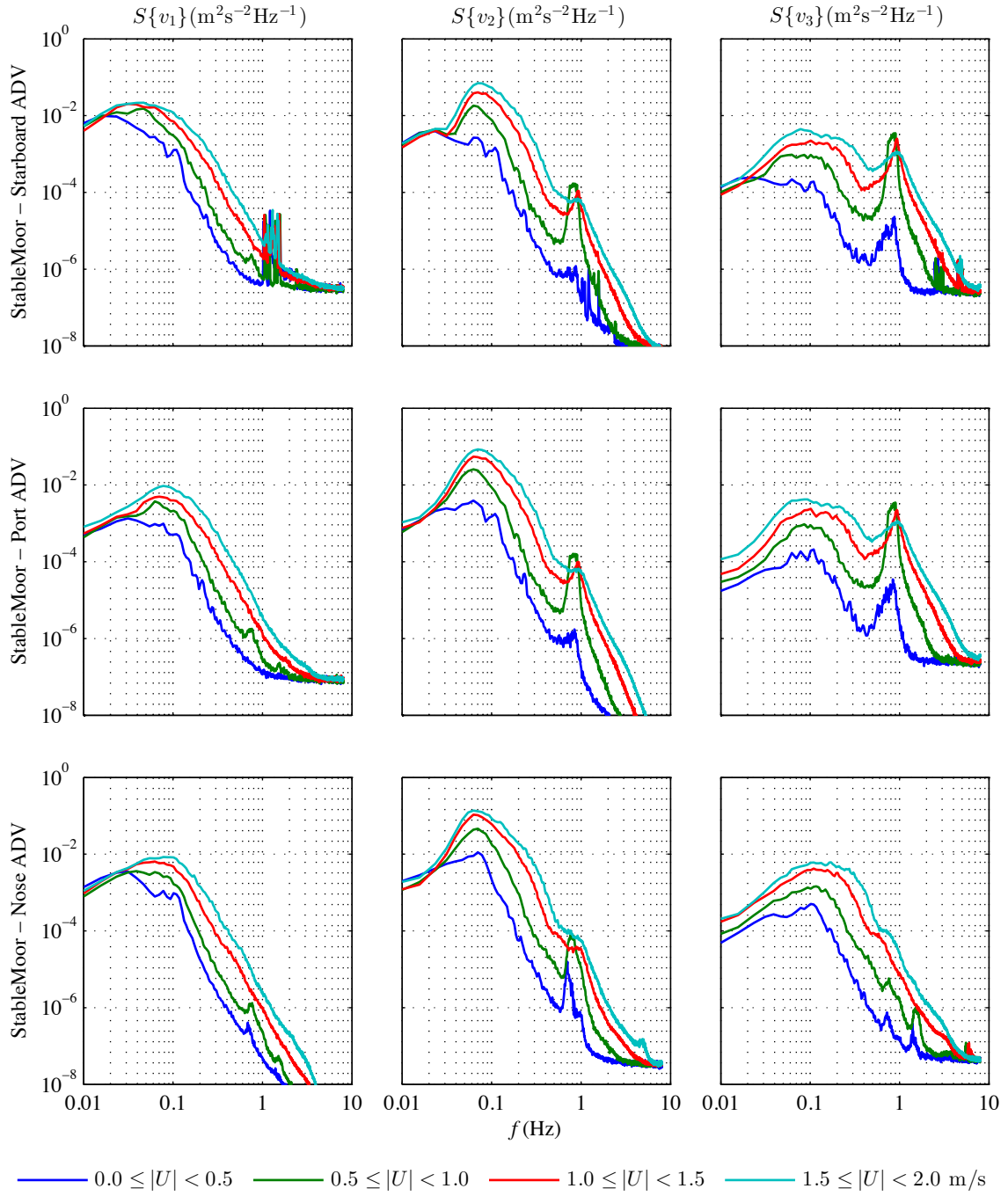


Figure 5: StableMoor motion for ADV deployments in winged mode (top and middle), and nose mode (bottom).

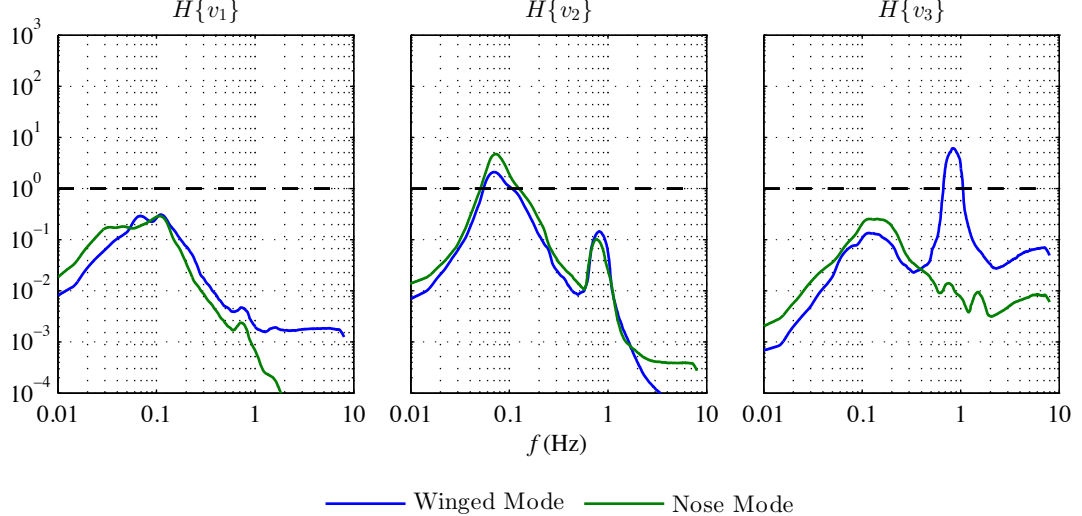


Figure 6: Frequency response amplitude of StableMoor ADV motion for velocity range $0 \leq U < 1 \text{ ms}^{-1}$ for starboard ADV in winged mode and nose ADV.

185 system. The ability of the ADV mounting board to yaw about the mooring
 186 line also introduces a lateral motion of the ADV head. The frequency re-
 187 sponse amplitude calculated for the motion of the TTM system is presented
 188 in Figure 7.

189 The dominant motion of the system, particularly at low flow speeds,
 190 results from the vortex induced velocity (VIV) of the large spherical mooring
 191 buoy at the end of the mooring line (Figure 3c). This configuration can
 192 be interpreted as a buoyant pendulum system, with a natural frequency
 193 described as a function of the Strouhal number of the spherical buoy, S_n ,
 194 by Equation 3.

$$f_n = \frac{US_n}{D} \quad (3)$$

195 After verifying that the drag force may be neglected, the Strouhal num-
 196 ber can be approximated to account for added mass by using Equation 4
 197 (Williamson and Govardhan, 1997; Govardhan and Williamson, 2005). Here
 198 $Fr = U/\sqrt{gD}$, m^* is the sphere mass normalized by the displaced mass of
 199 fluid ($m^* = m/(\frac{1}{6}\pi D^3 \rho)$), and C_A is the added mass coefficient equal to 0.5.

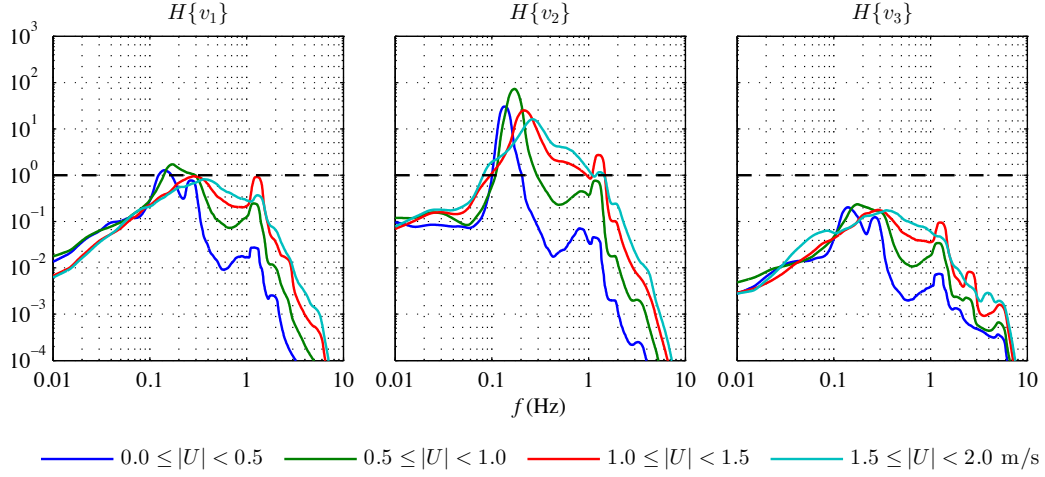


Figure 7: TTM frequency response amplitude

$$S_n \approx \frac{1}{2\pi Fr \sqrt{L/D}} \sqrt{\frac{1 - m^*}{C_a + m^*}} \quad (4)$$

By substituting Equation 4 into Equation 3, the theoretical natural frequency of the buoyant spherical pendulum is calculated as 0.13 Hz. The peak motion frequencies measured in the lateral direction are in the range of 0.10 – 0.25 Hz. The comparable frequencies of this motion is interpreted as confirmation of the *a priori* assumption of vortex-induced motion of the spherical buoy.

The higher frequency motion-induced ADV velocities measured in the lateral direction is attributed to the ability for the ADV vane to yaw about the mooring line in a fluttering motion. As such, the stream-wise and vertical motion at this frequency are significantly lower than the transverse motion. Evidence of motion in these directions at the same frequency is due to the mooring line deviating from vertical due to blow-down of the TTM system to an angle of 20° at mean flow speeds of 2.0 ms⁻¹ (Thomson et al., 2013).

4.1.3. Sounding weight

The frequency response amplitudes of the motion-induced velocity of sounding weight ADV are presented in Figure 8. The sounding weight was deployed from the research vessel as it was holding station in flow speeds of $1.0 < U \leq 1.5$ ms⁻¹. The port deployments used the davit for deployment

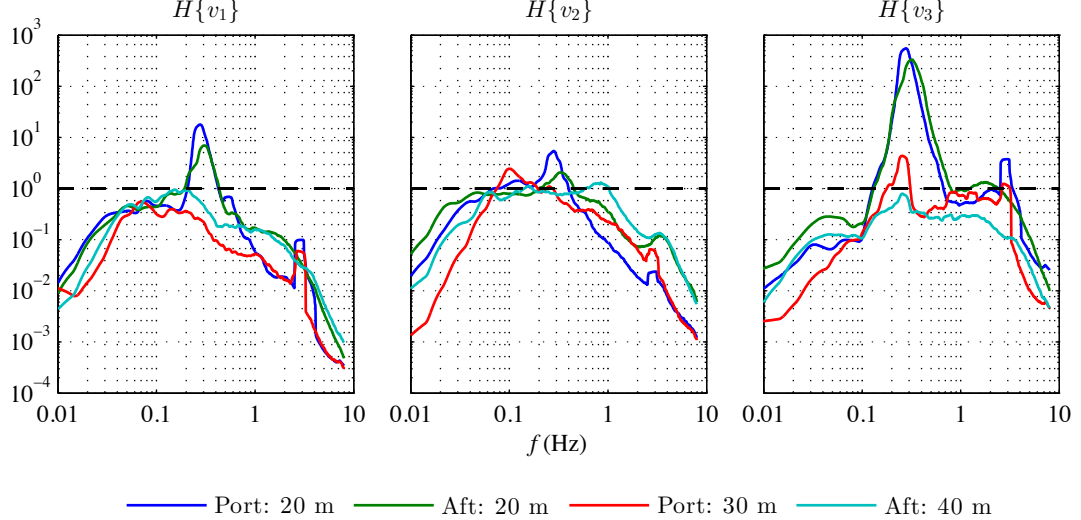


Figure 8: Comparison of sounding weight

with a thin line. The aft deployments utilized the A-frame winch, with a relatively thick tethering line.

The primary motion of the sounding weight is a pitching-heaving dynamic at a frequency of $f \approx 0.27$ Hz. The amplitude of this motion is significantly greater at the shorter line lengths of 20 m, and decreases as the line length is increased. The angle of the line was seen to increase with line length which may also be responsible for some change in motion dynamics. The port deployment shows greater motion than the aft, which may be due to the thicker tethering line providing increased motion damping in the latter.

Neglecting the effect of added mass and drag allows the deployed sounding weight to be modeled as a pendulum with the frequency of Equation 5, where T is equal to the tension in the line after accounting for buoyancy effects (Govardhan and Williamson, 1997).

$$f_n \approx \frac{1}{2\pi} \sqrt{\frac{T}{mL}} \quad (5)$$

Using Equation 5, the theoretical natural frequencies for the line lengths of 20, 30 and 40 m are 0.11, 0.09 and 0.08 Hz, respectively. Though the frequency response amplitude of the sounding weight motion does not show a very steep resonance peak, the approximation of the peak frequency given

235 by Equation 5 is within the frequency range of maximum motion of $0.08 \leq$
236 $f \leq 0.4$ Hz in the transverse direction.

237 The motion of the sounding weight is subject to forcing terms not found
238 in the SMB and TTM. Firstly, the instrument is tethered to the research
239 vessel which is holding station in the unsteady flows and affected by surface
240 dynamics (waves and swell). This introduced an additional velocity source
241 not found in the seabed tethered systems. As a result of this deployment
242 method, the ADV may also be exposed to the prop-wash aft of the pro-
243 pellers, which is particularly significant for the shorter tethering lines and
244 instrument deployed from the aft rather than the port. The deployment of
245 each sounding weight was limited to between 30 – 60 minutes so the fre-
246 quency response of Figure 8 represents significantly less data than the SMB
247 and TTM deployments. While strumming was observed in the lines above
248 the water level, the frequency of this exceeds that captured by the ADV-IMU
249 and the resulting motion-induced velocity at the ADV head is expected to
250 be negligible. The combination of these factors make direct comparison of
251 the sounding weight with the SMB and TTM deployments difficult.

252 5. Platform motion comparison

253 The ADV motion of a range of platform configurations discussed herein is
254 presented in Figure 9. These spectra represent the motion-induced velocities
255 at the ADV head for flow conditions in the range of $1.0 \leq U < 2.0$ ms⁻¹ as
256 the velocity range most relevant to the application of tidal energy.

257 In the stream-wise direction the SMB platform is significantly more stable
258 than the TTM at $f > 0.1$ Hz, with an order of magnitude reduction in motion
259 induced velocities for $f > 1.0$ Hz. This high frequency stability is comparable
260 in the transverse direction. Though there is evidence of the SMB natural
261 frequency at $f \approx 0.8$ Hz the motion-induced velocities remain significantly
262 lower than the TTM platform. This is particularly significant in the context
263 of turbulence measurements which utilize the higher frequency capabilities
264 of the ADV to characterize the inertial sub-range.

265 The TTM is at least as stable as the SMB and sounding weight at lower
266 frequencies ($f < 0.1$ Hz) in all directions. However at frequencies above the
267 threshold, the motion induced velocity of the TTM ADV in the stream-wise
268 and lateral directions is the greatest of all the platform configurations shown.
269 In particular, the VIV frequency of the spherical buoy causes a peak in the
270 motion of the TTM at $f \approx 0.13$ Hz.

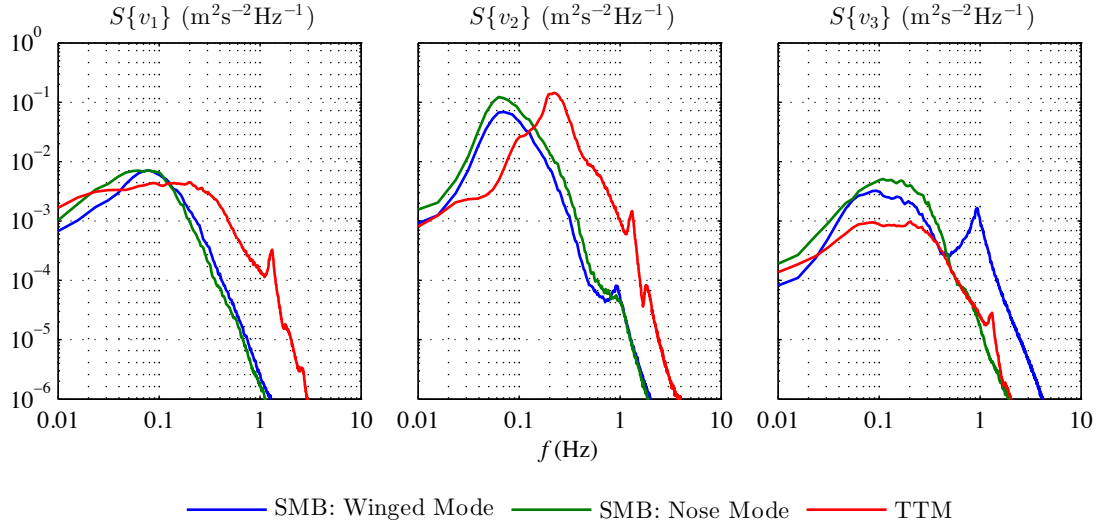


Figure 9: Motion-induced ADV velocity spectra for range of instrumentation platforms and configurations.

271 However, the TTM is the most stable platform at all frequencies in the
 272 vertical direction. This is particularly important in the use of ADVs to
 273 characterize turbulence, because the vertical component of velocity is the
 274 cleanest measurement from the ADV head in the configurations deployed as
 275 a result of the beam geometry. As a result, for isotropic turbulence, this
 276 velocity component provides the best estimate of TKE dissipation rate via
 277 the inertial sub-range. The TTM is therefore the most appropriate mooring
 278 for this use, though its performance is inferior in the other directions of
 279 motion.

280 6. Conclusions

281 Tethered instrumentation platforms are able to be used to deploy ADVs
 282 in energetic tidal environments through the development of motion correc-
 283 tion calculations introduced in Part 1 of this paper. However, large motion-
 284 induced velocities at the ADV head can result in persistent motion contami-
 285 nation of the corrected velocity signal. The platform motions analyzed show
 286 that the frequency response is sensitive to the flow speed and the platform
 287 geometries and configurations.

288 To summarize, the SMB with a single ADV deployed on the nose provided

289 the most stable ADV measurement, with superior frequency response at $f >$
290 0.1 Hz. This resulted in an uncontaminated motion-corrected measurement
291 of the velocity spectra throughout the inertial sub-range of the turbulence
292 measurement. When the SMB was deployed in wing mode, the roll of the
293 platform induced a significant vertical velocity component at the ADV-head
294 at $f \approx 0.8$ Hz. While providing a stable platform at **relatively low frequencies**
295 ($f < 0.1$ Hz) and in the vertical direction, the motion at the TTM ADV was
296 an order of magnitude larger than that of the SMB in the stream-wise and
297 transverse directions for most of the frequencies corresponding to the inertial
298 sub-range turbulence at the deployment site.

299 The performance of the sounding weight platform showed a very large
300 oscillatory component in the vertical direction for the 20 m deployments as
301 the platform became unsteady in pitch. For the case of the sounding weight,
302 the induced motion is a function of both the platform dynamics and the
303 vessel motion to which it is coupled. The resulting motion contamination is
304 the largest for all the platforms considered in these tests over most of the
305 frequency range considered.

306 7. Acknowledgments

307 The authors would like to thank Joe Talbert and Alex de Klerk for the
308 fabrication and preparation of the moorings as well as engineering support
309 during the field operations. The authors thank Capt. Andy Reay-Ellers for
310 his assistance in the precise deployment and retrieval of mooring hardware.

311 References

- 312 Afgan, I., McNaughton, J., Rolfo, S., Apsley, D. D., Stallard, T., Stansby,
313 P., 2013. Turbulent flow and loading on a tidal stream turbine by LES and
314 RANS. International Journal of Heat and Fluid Flow 43, 96–108.
- 315 Edson, J. B., Hinton, A. A., Prada, K. E., Hare, J. E., Fairall, C. W., 1998.
316 Direct Covariance Flux Estimates from Mobile Platforms at Sea. Journal
317 of Atmospheric and Oceanic Technology 15 (1991), 547–562.
- 318 Govardhan, R., Williamson, C., 1997. Vortex-induced motions of a tethered
319 sphere. Journal of Wind Engineering and Industrial Aerodynamics 69-71,
320 375–385.

- 321 Govardhan, R. N., Williamson, C. H. K., 2005. Vortex-induced vibrations of
322 a sphere. *Journal of Fluid Mechanics* 531, 11–47.
- 323 Kilcher, L., Thomson, J., Colby, J., 2014a. Determining the spatial coherence
324 of turbulence at MHK sites. In: 2nd Marine Energy Technology Sympo-
325 sium. Seattle, WA.
- 326 Kilcher, L., Thomson, J., Talbert, J., Deklerk, A., 2014b. Measuring turbu-
327 lence from moored acoustic Doppler velocimeters: A manual to quantifying
328 inflow at tidal energy sites. Tech. rep.
- 329 Legrand, C., 2009. Assessment of Tidal Energy Resource. Tech. rep., Euro-
330 pean Marine Energy Centre Ltd.
- 331 LORD MicroStrain, 2014. LORD Datasheet: 3DM-GX3-25-OEM, OEM At-
332 titude Heading Reference System (AHRS).
- 333 Matt, S., Hou, W., Woods, S., Goode, W., Jarosz, E., Weidemann, A., 2014.
334 A novel platform to study the effect of small-scale turbulent density fluc-
335 tuations on underwater imaging in the ocean. *Methods in Oceanography*
336 11 (2014), 39–58.
- 337 McCann, G., 2007. Tidal current turbine fatigue loading sensitivity to waves
338 and turbulence a parametric study. In: 7th European Wave and Tidal
339 Energy Conference. Porto, Portugal.
- 340 Milne, I., Sharma, R., Flay, R., Bickerton, S., 2010. The Role of Onset
341 Turbulence on Tidal Turbine Blade Loads. In: 17th Australasian Fluid
342 Mechanics Conference.
- 343 Paskyabi, M. B., Fer, I., 2013. Turbulence measurements in shallow water
344 from a subsurface moored moving platform. *Energy Procedia* 35 (January),
345 307–316.
- 346 Polagye, B., Thomson, J., 2013. Tidal energy resource characterization:
347 methodology and field study in Admiralty Inlet, Puget Sound, WA (USA).
348 Proceedings of the Institution of Mechanical Engineers, Part A: Journal of
349 Power and Energy 227 (3), 352–367.
- 350 Thomson, J., Kilcher, L., Richmond, M., Talbert, J., DeKlerk, A., Po-
351 lagye, B., Guerra, M., Cienfuegos, R., 2013. Tidal turbulence spectra

- 352 from a compliant mooring. In: 1st Marine Energy Technology Symposium
353 (METS2013). Washington, D.C.
- 354 Thomson, J., Kilcher, L. F., Harding, S., 2014. Multi-scale coherent tur-
355 bulence at tidal energy sites. In: 5th International Conference on Ocean
356 Energy (ICOE2014). Halifax, Nova Scotia, pp. 1–6.
- 357 Williamson, C. H. K., Govardhan, R., 1997. Dynamics and Forcing of a
358 Tethered Sphere in a Fluid Flow. Journal of Fluids and Structures 11,
359 293–305.

360 **Appendix A. Combined motion spectra of ADV-IMU and ADCP-**
361 **BT**

362 *Appendix A.1. Introduction*

363 The motion of a tethered instrumentation platform was recorded using
364 two methods of measurement; an inertial measurement unit (IMU) integrated
365 with an acoustic Doppler velocimeter (ADV), and the bottom-tracking (BT)
366 functionality of an acoustic Doppler current profiler (ADCP). The IMU motion
367 is recorded at relatively high frequency but is unable to capture low
368 frequency linear velocities due to the inherent signal drift of the integral of
369 the measured acceleration. Conversely, the ADCP-BT is unable to capture
370 high frequency motions (above the order of $f = 1$ Hz) due to the limitations
371 in ping frequencies of the profiling instrument. This appendix outlines the
372 process of combining the high frequency ADV-IMU motions with the low
373 frequency ADCP-BT to calculate the motion-induced velocity spectra at the
374 location of the ADCP, over a wide range of frequencies. An IMU-equipped
375 ADV, and BT-capable ADCP were deployed on the tethered StableMoor in-
376 strumentation platform in Admiralty Inlet, WA for 24 hours from 12:00 on
377 the 12th May 2015. The locations of the ADV and ADCP on the StableMoor
378 platform are shown in Figure 2.

379 Bench-tests of the Microstrain IMU indicate that its accelerometers drift
380 for frequencies less than 0.01 Hz. Therefore, in order to remove bias-drifts
381 which cause large errors in \vec{u}_a , the measured $\vec{a}'(t)$ has been high-pass fil-
382 tered with a threshold of $f_a = 0.033$ Hz (30 seconds) (Kilcher et al., 2014b).
383 As a result, real motions at and below f_a will be underestimated using the
384 ADV-IMU method.

385 The bottom-tracking method of the ADCP calculates the platform motion
386 using the Doppler shift of acoustic pulses reflected from the seabed. The
387 sample frequency of this method is limited to the order of $f = 1$ Hz, to avoid
388 signal contamination due to ringing in the transducer head. The BT mea-
389 surements are compensated for rotation-induced motion using the orientation
390 sensors of the instrument. As such, the BT measurement represents the low
391 frequency motion of the SMB at the ADCP location.

392 In this way, both the ADV-IMU and ADCP-BT can independently detect
393 the motion of the tethered platform at the location of the ADCP within a
394 limited frequency range, as shown for the transverse direction in Figure A.10.
395 This plot shows some agreement between the two methods of measurement
396 within the frequency band of $0.1 < f < 0.3$ Hz.

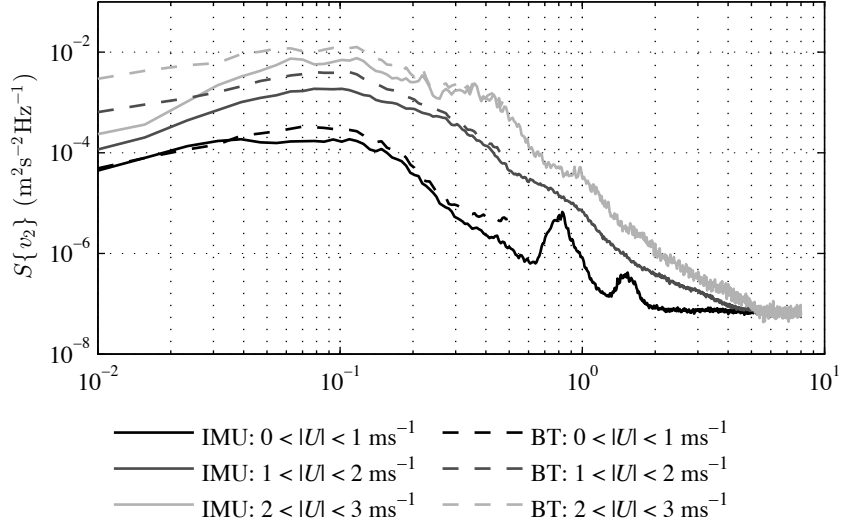


Figure A.10: Spectra of vertical ADCP motion in platform coordinate systems, using ADV-IMU and ADCP-BT methods for a number of mean flow velocities.

397 This appendix describes how the output of these instruments can be com-
 398 bined to calculate the motion of the platform, at the location of the ADCP,
 399 over a wider range of frequencies than using the ADV-IMU alone.

400 *Appendix A.2. Methods*

401 The following subsections outline the process of combining the ADV-IMU
 402 and ADCP-BT data sets to calculate the full spectra of platform motion. The
 403 following analysis is performed with all velocities in the platform coordinate
 404 system.

405 *Appendix A.2.1. Clock synchronization*

406 Accurate clock synchronization is required in order to combine the motion
 407 signals of the two instruments. Though both instruments were synchronized
 408 with GPS time during the week of deployment, clock drift was observed on
 409 the order of two seconds per day. Using the ADV clock as the reference
 410 time signal, the time difference of the ADCP was calculated using the cross-
 411 correlation of the vertical velocity time series, $z(t)$, using the following steps.

- 412 • Interpolate the BT velocity time series from the sample frequency of 1
 413 Hz to the IMU frequency of 16 Hz.

- 414 ● Divide the time series of both the IMU and BT derived motion into
 415 120 s sub-series and calculate the time difference associated with the
 416 peak cross-correlation of each 120 s sub-series.
- 417 ● Filter the spurious clock differences calculated at the slack tides, where
 418 the motion signal and resulting correlation was insufficient to detect
 419 significant cross-correlation.
- 420 ● Fit a linear trend line to the clock difference as a function of time and
 421 calculate the offset and gain of the ADCP clock, relative to the ADV.
- 422 ● Adjust the raw clock signal of the ADCP time series using the linear
 423 regression coefficients.

424 The ADCP clock began with an offset of 2.8 s, and drifted by 0.07 s per
 425 hour relative to the ADV clock.

426 *Appendix A.2.2. Frequency response filter*

427 Before the motion signals of the ADV-IMU and ADCP-BT methods can
 428 be combined, the signals must be attenuating using complementary filters
 429 such that the sum of the filter amplitudes is unity at all frequencies.

430 This achieved by using filter transfer functions which are symmetrical
 431 about the threshold frequency. The filter used in this analysis is a first-order
 432 Butterworth filter. The low-pass Butterworth filter is applied to the ADCP-
 433 BT motion, and the high-pass equivalent is applied to the the ADV-IMU
 434 motion.

435 Note that this high-pass filter has already been applied to the linear mo-
 436 tion (not rotation-induced) component of the ADV-IMU motion in the *dolfyn*
 437 toolbox. Therefore, it is only applied to the rotation-induced component at
 438 this stage.

439 *Appendix A.3. Results*

440 The rotated motion vectors of each instrument were confirmed to have the
 441 same sign in the platform coordinate system. As such, the synchronized and
 442 filtered time-series of the platform motion were summed in the time domain.
 443 The spectra of the filtered motions from each instrument and the resulting
 444 combined motion signal is shown in Figure A.11.

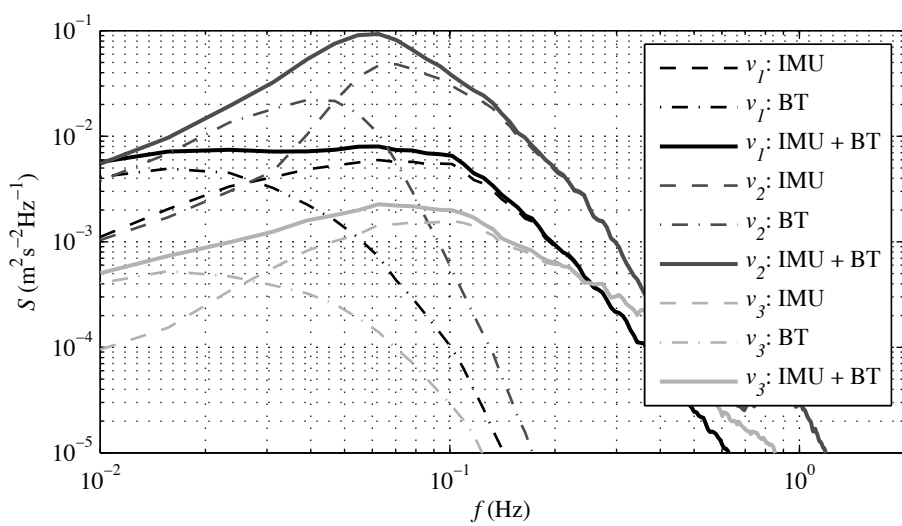


Figure A.11: Spectra of the combined filtered motion signals